Improved OSIRIS NO₂ retrieval algorithm: Description and validation

Christopher E. Sioris[1], Landon A. Rieger[2], Nicholas D. Lloyd[2], Adam E. Bourassa[2], Chris Z. Roth[2], Douglas A. Degenstein[2], Claude Camy-Peyret[3], Klaus Pfeilsticker[4], Gwenaël Berthet[5], Valéry Catoire[5], Florence Goutail[6], Jean-Pierre Pommereau[6], and Chris A. McLinden[1]

[1]{Air Quality Research Division, Environment Canada, Toronto, Canada}

[2]{University of Saskatchewan, Saskatoon, Canada}

[3]{Institut Pierre Simon Laplace, France}

[4]{Institute of Environmental Physics, University of Heidelberg, Heidelberg, Germany}

[5]{Centre National de la Recherche Scientifique, Orléans, France}

[6]{Centre National de la Recherche Scientifique, Guyancourt, France}

Correspondence to: Christopher.Sioris@canada.ca

Abstract

A new retrieval algorithm for OSIRIS (Optical Spectrograph and Infrared Imager System) nitrogen dioxide (NO₂) profiles is described and validated. The algorithm relies on spectral fitting to obtain line-of-sight (LOS) column densities of NO₂ followed by inversion using an algebraic reconstruction technique and the SaskTran spherical radiative transfer model to obtain vertical profiles of local number density. The validation covers different latitudes (tropical to polar), years (2002-2012), all seasons (winter, spring, summer, and autumn), different concentrations of nitrogen dioxide (from deNOxified polar vortex to polar summer), a large range of solar zenith angles (68.6 to 90.5°) and altitudes between 10.5 and 39 km, thereby covering the full retrieval range of a typical OSIRIS NO₂ profile. The use of a larger spectral fitting window than used in previous retrievals reduces retrieval uncertainties and the scatter in the retrieved profiles due to noisy radiances. Improvements are also demonstrated through the

1   validation in terms of bias reduction at 15-17 km relative to the OSIRIS operational v3.0

2   algorithm. By accounting for the diurnal variation along the LOS in the two-dimensional

3   radiative transfer model, the scatter of the differences relative to the correlative balloon NO_2

4   profile data is reduced.

5   **1. Introduction**

6   Nitrogen oxides, such as NO and NO_2 are the reactive nitrogen-containing species in the middle

7   atmosphere and are produced mainly from the breakdown of nitrous oxide in the stratosphere.

8   Oxides of nitrogen dominate ozone loss in the middle stratosphere, whereas in the lower

9   stratosphere, they react with oxides of chlorine and bromine, such as ClO and BrO, to reduce the

10   halogen-catalyzed destruction of ozone.

11   The partitioning between NO and NO_2 depends on several factors such as the local ozone

12   concentration and the photolysis frequency of NO_2. Reactive nitrogen is chemically converted at

13   night to N_2O_5 and, upon hydrolysis, can be further sequestered into unreactive 'reservoir' species

14   such as HNO_3. NO_2 increases steadily during daylight hours due to the UV photolysis of N_2O_5

15   (e.g. Wetzel et al., 2012).

16   The photochemistry of NO_2, which is particularly rapid near the day-night terminator, leads to

17   spatial gradients within the field of view, particularly for limb sounders such as OSIRIS (Optical

18   Spectrograph and Infrared Imager System) (Llewellyn et al., 2004), or for solar occultation

19   instruments operating in either the UV-visible or mid-infrared (e.g., Kerzenmacher et al., 2008).

20   The OSIRIS operational NO_2 retrieval algorithm was developed and validated by Haley and

21   Brohede (2007) and the current version is 3.0. The work of Kerzenmacher et al. (2008) is the

22   only other publication comparing version 3.0 OSIRIS NO_2 data to correlative profile

23   measurements. Earlier versions (e.g., 2.x, Haley et al., 2004) were more thoroughly validated, for

24   example by Brohede et al. (2007). The pseudo-spherical forward model used in the operational

25   OSIRIS NO_2 retrieval algorithm is less accurate than the SaskTran spherical radiative transfer

26   model (RTM, Bourassa et al., 2008, Zawada et al., 2015), currently used as a forward model in

27   the operational retrieval algorithm for OSIRIS ozone and aerosol extinction data products.

28   Recently, Bourassa et al. (2011) developed an alternative NO_2 algorithm which relied on 4

29   wavelengths covering a single NO_2 absorption band. This was later modified to 13 wavelengths

1   covering three adjacent NO_2 bands (438-450 nm) and used to process the entire OSIRIS data

2   record and is referred to here as the 'fast' OSIRIS NO_2 product. While the spectral information

3   content is reduced relative to the operational OSIRIS algorithm and the algorithm described

4   below (see Table 1), the 'fast' algorithm has two key common elements to the one described

5   herein:

6   1) The forward model is the successive-orders-of-scattering version of SaskTran.

7   2) MART (Multiplicative Algebraic Reconstruction Technique) (Degenstein et al., 2003) is

8   used for inversion.

9   In this work, we provide a detailed description of the new retrieval algorithm whose heritage is

10   the 'fast' algorithm (Bourassa et al., 2011) as well as the algorithm developed in a series of

11   papers (Sioris et al., 2003; Sioris et al., 2004; Sioris et al., 2007). The current algorithm was

12   developed to demonstrate that improved accuracy is possible through the combination of a better

13   forward model, better forward model inputs, and additional, longer wavelengths, with a

14   particular focus on the lower stratosphere (and upper troposphere).

15   We then compare NO_2 profiles retrieved from OSIRIS observations to balloon-borne NO_2 profile

16   measurements during the decade (2002-2012) when several balloon-borne limb measurements

17   were performed. Balloon profiles are chosen for the validation for many reasons, of which the

18   most important is the expected accuracy of this data. The accuracy is due to two main factors:

19   very high signal-to-noise afforded by the luxury of long exposure times (which can be traded for

20   higher vertical and/or spectral resolution) and superior altitude determination, which for balloon-

21   borne limb geometry is due to the sensor being an order of magnitude closer to the tangent point

22   than for satellite limb sounders, thereby reducing the impact of imperfect viewing angle

23   knowledge. Profile measurements from balloons are preferable to those from satellite for the

24   purpose of validation because of their high vertical resolution, generally matching or exceeding

25   the ~2 km vertical resolution of OSIRIS NO_2 (e.g. Sioris et al., 2003) (see below). Balloon

26   measurements exploit a greater diversity of methods as in-situ techniques are possible in addition

27   to remote sensing. Furthermore, one balloon-borne remote sensing technique relies on

28   occultation during balloon ascent/descent, which is not possible for satellite instruments, and

29   provides very accurate altitude registration, offers potentially finer vertical resolution than limb

1 occultation for instruments observing the full solar disk (see Sect 2.3) and smaller errors due to

2 the neglect of diurnal NO_2 gradients.

2. Method

2.1 Algorithm settings

5 The algorithm is a classic 2-step approach of spectral fitting using absorption cross-sections to

6 determine slant column densities (SCDs) and vertical fitting to invert the SCDs. This approach is

7 used by many groups including some of the balloon remote sensing teams providing data used in

8 this study. The reference spectrum is the co-addition of spectra at tangent heights (THs) in the

9 50-70 km range (Sioris et al., 2003). Spectral fitting refers to a multiple linear regression

10 including the following basis functions: a fourth order closure polynomial which is justified

11 based on an adjusted-R^2 test, and temperature-dependent NO_2 (Vandaele et al., 1998) and O_3

12 (Serdyuchenkov et al., 2014) absolute absorption cross sections interpolated to the temperature

13 (T) of the tangent layer using the European Centre for Medium-Range Weather Forecasting

14 (ECMWF) analysis and convolved with a Gaussian to OSIRIS spectral resolution. Water vapour

15 absorption is neglected despite maximal absorptions of >0.1% in the fitting window (434.8-476.7

16 nm) in the upper troposphere as it is not spectrally correlated with NO_2 absorption over this

17 window and would greatly increase the forward modelling computational burden. The spectral

18 fitting is exactly the same for observed and simulated normalized radiances. For example, the

19 actual OSIRIS wavelengths and tangent heights are inputs into the simulation and any spectral

20 pixels which are rejected due to radiation hits or detector saturation at the Level 1 processing

21 stage (i.e. observed radiances) are also omitted from the fit of the SaskTran-simulated radiances.

22 The longest wavelength in the fitting window is extended to 476.7 nm, raising the number of

23 spectral pixels to 107, thereby increasing the spectrally-integrated signal-to-noise ratio and the

24 penetration of the lower atmosphere relative to both existing OSIRIS NO_2 algorithms mentioned

25 above. Both of these benefits of an extended fitting window had been demonstrated for

26 SCIAMACHY limb scattering (Sioris et al., 2004) but OSIRIS has a glass filter that prevents the

27 detection of higher orders of light reflected off the grating that was positioned such that the 477-

28 530 nm region is not usable (Warshaw et al., 1996). Thus the 434.8-476.7 nm window is used

29 here and spectral fitting residuals are shown in Fig. 1. Using a discontinuous fitting window that

30 included wavelengths greater than 530 nm is not beneficial. The NO_2 SCD uncertainties are

1 improved relative to those obtained by Sioris et al. (2003) who used a 434.8-449.0 nm fitting

2 window and the 'tilt' pseudo-absorber. The improved NO_2 number density precision is illustrated

3 below. The 'tilt' basis function is now excluded from the spectral fitting. We also tested an

4 alternative approach of fitting an NO_2 spectral weighting function to the normalized radiances, as

5 is used to fit the ozone absorption signal in nadir reflectance spectra (Coldewey-Egbers et al.,

6 2005) and the spectral fits did not improve significantly.

7 The retrieval upper altitude limit is defined by the lowest tangent height in a limb scan for which

8 the NO_2 SCD error is <100% for all tangent heights below. This can be as high as 49 km, but is

9 typically ~40 km and typically a few kilometres higher than the upper altitude of the 'fast' NO_2

10 product. The lower limit of the retrieval is often determined by cloud tops as Odin generally

11 scans the limb into the upper troposphere. Cloud-contaminated observations are excluded as they

12 can lead to biases and difficulty in retrieval convergence. Cloud top detection is particularly

13 important for MART since spectra from successive tangent heights immediately below a given

14 altitude are used in a weighted fashion to retrieve the NO_2 number density at that altitude. We

15 assume, for OSIRIS geometry (scattering angles of $90\pm30°$), that an observed scene near a cloud

16 top sampled by the ~1 km tall instantaneous-field-of-view has larger limb radiance at ~810 nm

17 than if it were cloud-free. A scene is deemed to be cloudy if the ~810 nm radiance scale height is

18 < 2.4139. This threshold is lowered from an overly stringent value of 3.84 (Sioris et al., 2007).

19 The new threshold is chosen to allow NO_2 retrievals (and validation) to extend below 2-3 month

20 old volcanic aerosol layers due to Sarychev Peak and Nabro, two of the eruptions during the

21 OSIRIS mission which led to the largest stratospheric aerosol optical depth.

22 Algebraic reconstruction techniques (Fesen and Hays, 1982) have been used to recover the

23 vertical and along-track distribution of atmospheric constituents for over four decades (Thomas

24 and Donahue, 1972). Chahine's (1968) relaxation method, used by Sioris et al. (2007) for the

25 retrieval of OSIRIS NO_2 vertical profiles, is a variant of MART in which only the tangent layer

26 is used to retrieve the local number density and is also tested (see Sect. 4). The MART retrieval

27 in this work uses a 0.6:0.3:0.1 weighting following the OSIRIS aerosol extinction retrieval (see

28 Eq. 8 of Bourassa et al., 2007). Exactly 15 retrieval iterations are used, which appears to be

29 adequate for most cases and, with MART, does not lead to overfitting. Five orders of scattering

30 are used (Sioris et al., 2004). The retrieval uses a 1 km altitude grid, although the NO_2 vertical

1 resolution remains ~2 km, a consequence of the ~2 km vertical sampling provided by Odin.

2 Above the retrieval range, NO_2 profiles are scaled every iteration using a Chahine-like update

3 based on the highest tangent height within the retrieval range. Below the retrieval range, the NO_2

4 profile is assumed to have a constant number density down to the ground, equal to the number

5 density at the lowest retrieved altitude. The air number density profile is from ECMWF.

6 The retrieval uses OSIRIS-retrieved ozone and aerosol extinction profiles (version 5.07, v5.07

7 hereafter) and the 675 nm scene albedo (Bourassa et al., 2007) to provide more realistic forward

8 model inputs into SaskTran.

9 The NO_2 retrieval uncertainty is obtained by perturbation as described by Sioris et al. (2010),

10 with the NO_2 SCD standard errors and an altitude-independent number density perturbation

11 serving as inputs. The 1D profile retrieval including the error calculation takes ~5 minutes on a

12 desktop computer with eight 3.4 GHz processors.

13 ## 2.2.   Modelling diurnal gradients within SaskTran

14 Zawada et al. (2015) describe the high spatial resolution capability which is required for

15 modelling (horizontal) diurnal gradients of NO_2 within SaskTran. SaskTran is capable of

16 modelling radiation fields with the atmosphere varying along the line-of-sight (LOS), and also

17 along the incoming solar beam (referred to as '2D mode' and '3D mode', respectively,

18 hereafter). The 1D forward model and associated retrieval (Table 1) completely neglects diurnal

19 gradients in NO_2. In 2D mode, the atmosphere consists of sectors along the LOS but the diurnal

20 variation of NO_2 along the incoming solar beam is not considered. In 3D mode, the atmosphere

21 essentially consists of stacked triangular prisms of increasing horizontal extent with increasing

22 distance from the tangent point as illustrated by Zawada et al. (2015) and diurnal gradients are

23 simulated for any light path from its point of entry into the atmosphere to its exit.

24 To provide realistic diurnal gradients in the atmosphere of the forward model, SaskTran has been

25 linked to the PRATMO stratospheric gas-phase photochemical box model (McLinden et al.,

26 2000). PRATMO is configured to converge to 0.5% between the start and end of each one day

27 run. The atmosphere is aerosol-free for photolysis frequency calculations. The latitudinal and

28 vertical resolutions are 5° and ~2 km, respectively. The default number of time steps per day is

29 35. More details are available in McLinden et al. (2006) and references therein.

1   **2.3 Validation approach and datasets**

2   Even though the OSIRIS 2D and 3D profiles are retrieved accounting for the diurnal gradients

3   expected for the OSIRIS viewing geometry, photochemical modelling is also required to scale all

4   of the OSIRIS NO_2 profiles to the local time of the balloon measurement. The PRATMO box

5   model is also used for this purpose.

6   Balloon correlative data are used from the following instruments:

7   Differential Optical Absorption Spectroscopy (DOAS, Butz et al., 2006; Kreycy et al., 2013, and

8   references therein), miniDOAS (Weidner et al., 2005), Limb Profile Monitor of the Atmosphere

9   (LPMA, Butz et al., 2006), Spectromètre Infra-Rouge d'Absorption par Lasers Embarqués

10   (SPIRALE, Kerzenmacher et al., 2008; Moreau et al., 2005), Système d'Analyse par Observation

11   Zénithale (SAOZ, Pommereau and Piquard, 1994; Wetzel et al., 2007), SAOZ-BrO (Pundt et al.,

12   2002), mini-SAOZ (Vicomte and Pommereau, 2011), MkIV (Toon et al., 2002), and

13   Spectroscopie d'Absorption Lunaire pour l'Observation des Minoritaires Ozone et NO_x –

14   Nacelle 2 (SALOMON-N2) operating in solar occultation mode (Jégou et al., 2013). Table 2

15   provides information on these correlative datasets. The five balloon-borne instruments not

16   previously used in OSIRIS NO_2 validation are LPMA, miniDOAS, SPIRALE, SALOMON-N_2

17   and MkIV. DOAS and SAOZ had been used previously (Brohede et al., 2007; Haley et al., 2004;

18   Sioris et al., 2003). SPIRALE, LPMA, and SALOMON-N2 data were obtained from the

19   CNES/CNRS-INSU Ether web site (http://www.pole-ether.fr).

20   Coincidence criteria are within 1000 km (Brohede et al., 2007) and on the same calendar day

21   (using UT time). Only daytime correlative measurements are considered. The closest spatial

22   coincidence is used if located within a 1000 km range. Comparisons between OSIRIS NO_2 and

23   balloon correlative data are performed only down to the lower altitude limit of each profile

24   retrieved with the v3.0 algorithm in an effort to keep the number of balloon-coincident altitudes

25   the same between that algorithm and the algorithm debuting here. The upper limit for validation

26   is determined in all cases by the balloon float altitude.

27   The best opportunities for validation of a deNOxified profile come on March 4th and 16th, 2003

28   in Kiruna, Sweden when the NO_2 number density measured by LPMA and SAOZ, respectively,

29   did not exceed 10^9 molec/cm^3 at any altitude. These peak number densities are the lowest in the

1   validation dataset. Note that OSIRIS does not measure in the northern polar region until late

2   February due to a lack of sunlight at ~6 AM/PM. NO_2 profiles at southern high-latitudes have

3   not been measured by balloon-borne instruments during the OSIRIS mission.

4   Averaging kernels are not taken into account since the vertical resolution is similar between the

5   NO_2 profiles from most of the selected validation instruments and from the three OSIRIS

6   algorithms, namely the operational v3.0, 'fast', and the algorithm described herein. Results from

7   the current algorithm will be treated separately for each of the forward model modes (1D, 2D,

8   and 3D) described in section 2.2.

9   In section 3, the 1D profiles used in the validation are those processed by a network of computers

10   (using a solar zenith angle cutoff of SZA<90°). The entire OSIRIS data record has now been

11   processed and is currently available at ftp://odin-osiris.usask.ca/Level2/NO2/ following

12   registration. One time-saving approximation is used to process the entire record: multiple

13   scattering (MS) is only calculated at 21 wavelengths corresponding to the peaks and troughs of

14   the NO_2 absorption cross-section across the spectral fitting window rather than the entire set of

15   107 wavelengths. The single-scattering radiances at the remaining 86 wavelengths are scaled by

16   the ratio of radiances between multiple scattering and single scattering simulations at these 21

17   wavelengths, linearly interpolated to the remaining wavelengths. The radiance error due to the

18   MS approximation is typically <0.05% at all wavelengths and all tangent heights used in the NO_2

19   retrieval.

3   Results

22   One difference in the method described above (Sect. 2) compared to previous OSIRIS NO_2

23   algorithms (Haley and Brohede, 2007; Bourassa et al., 2011) is the use of spectral information

24   from longer wavelengths. Two sources of random error in retrieved NO_2 are shot noise, a

25   consequence of the finite number of electrons generated by the detector by impingent limb-

26   scattered photons, as well as radiation hits by energetic particles (e.g. protons) that are not

27   filtered in the Level 1 data. The extended fitting window tends to reduce the susceptibility of the

28   retrieved NO_2 to these noise sources. Using the 1D inversion approach described above, the 33

29   OSIRIS limb scans used in validation are processed with the extended fitting window and the

1   one used in the operational algorithm (Haley and Brohede, 2007). The standard deviation in

2   retrieved NO_2 number density for each set (i.e. fitting window) is calculated over the common

3   altitude range for each of the 33 scans. Natural variability of NO_2 is identical since the same limb

4   scans and altitude ranges are used, so any difference in the standard deviation is due solely to the

5   different spectral fitting windows. Figure 2 shows the slight reduction in NO_2 variability at all

6   altitudes with the extended fitting window. Note that the NO_2 profiles retrieved from the two

7   fitting windows do not have a significant bias (± 1 standard error) between themselves, which

8   points to the self-consistency of NO_2 spectral cross-section between the two windows.

9   Other benefits of the extended fitting window are that the NO_2 retrieval uncertainty is improved

10   and the upper altitude limit of the retrieval moves slightly higher, as shown for a sample case in

11   Fig. 2. For this tropical case, only at the NO_2 number density minimum at 15.5 km is the current

12   retrieval unable to measure NO_2 with uncertainty of <100%, whereas with the fitting window of

13   the operational algorithm, the measurements are below the lower detection limit between 11.5

14   and 17.5 km and at 7.5 km (Fig. 2). The significant upper tropospheric NO_2 enhancement at ~10

15   km is also observed by the mini-SAOZ (not shown).

16   Figure 3 shows that the 1D retrieval overestimates NO_2 by 29% relative to the 3D one at 17.5

17   km. This overestimate is due to the larger NO_2 concentrations that are present on the far side of

18   the limb (yet neglected by a 1D model) for a SZA (86.6°) that is small enough to allow

19   significant far side contribution to the radiance. The increasing NO_2 gradient toward the far side

20   of the limb occurs because of the decreasing photolysis frequency of NO_2 with increasing SZA.

21   The 2D retrieval underestimates slightly since the slightly lower NO_2 concentrations along the

22   incoming solar beam are not included in that model version. The 3D retrieval clearly reduces the

23   bias versus SAOZ relative to the 1D case at altitudes below 18 km where the relative diurnal

24   gradients are expected to be largest. This improved precision is demonstrated below for a large

25   ensemble of profiles by contrasting the correlation of the 1D and 2D retrievals and the standard

26   error of the biases relative to coincident balloon data.

27   In order to compare the various OSIRIS NO_2 products to the balloon correlative data, all profiles

28   are linearly interpolated onto a 1 km grid (12.0 to 39.0 km) commonly used in the balloon data.

29   The 'fast' product tends to be limited in its vertical range at both extremes of the profile, not only

30   relative to the other OSIRIS NO_2 products but also relative to the coincident balloon profiles and

1   also the 'fast' retrieval is not available for some coincidences (Fig. 4). The sample size is ≥20

2   between 13 and 31 km for all OSIRIS NO_2 products and the validation discussion focusses

3   mostly on this altitude range.

4   The v3.0 operational OSIRIS NO_2 has proven to be of high quality in the 15 to 42 km range from

5   previous satellite intercomparisons (e.g. Haley and Brohede, 2007) and the same can also be

6   inferred for the upper troposphere from the ability to detect small lightning-generated NO_2

7   enhancements with the expected latitudinal and longitudinal distribution (e.g. Sioris et al., 2007).

8   Thus, in Fig. 5, we examine the standard error of the coincident profiles for OSIRIS and balloon

9   data to compare the variability of each dataset, similar to Kerzenmacher et al. (2008). The upper

10 altitude limit of the data obtained from balloons launched by CNES (Centre National d'Etudes

11 Spatiales) is 31±2 km (Table 2). This excludes MkIV and SAOZ-BrO. From 31 down to 28 km,

12 the balloon-borne NO_2 profiles show more scatter than any of the OSIRIS data products. This is

13 likely due to the need to assume the NO_2 vertical distribution above float altitude for the remote

14 sensors which is particularly problematic in the tropics where the NO_2 profile typically peaks at a

15 higher altitude than for the extratropics. A second factor is the smaller absorption signal for the

16 remotely-sensing balloon instruments due to the short path lengths when observing altitudes near

17 float. Below 16 km, the balloon data clearly exhibits less scatter than OSIRIS, thereby

18 quantitatively supporting the choice of balloon validation data for reasons discussed in Sect. 1.

19 Kerzenmacher et al. (2008) show that this is not true for NO_2 at ~15 km measured by the

20 (Atmospheric Chemistry Experiment) ACE satellite instruments versus OSIRIS v3.0 NO_2.

21 Between the three OSIRIS products, 'fast' exhibits the largest scatter at all altitudes, whereas the

22 2D algorithm described here offers noticeably less scatter between 15 and 20 km as compared to

23 the v3.0 product. The 3D algorithm takes 1.5 hours to retrieve a profile on the computer

24 specified above and thus the entire set of balloon-coincident OSIRIS limb scans was not

25 processed. The 2D algorithm takes half of the processing time of the 3D algorithm.

26 To determine if OSIRIS NO_2 is biased relative to the balloon data, we studied medians and

27 means of individual profile differences over all coincidences (as a function of altitude). These

28 results are shown in Figs. 6-7. It is clear that all of the OSIRIS NO_2 algorithms have a

29 statistically significant bias near the NO_2 peak (typically ~30 km). This overestimate near the

30 peak is similar to the overestimate by OSIRIS v3.0 relative to ACE Fourier Transform

1   Spectrometer and MAESTRO (Measurements of Aerosol Extinction in the Stratosphere and

2   Troposphere Retrieved by Occultation) which coincided with the NO_2 peak altitude. Local biases

3   were +17% and 14%, respectively (Kerzenmacher et al., 2008). Haley and Brohede (2007) found

4   no such overestimate at the peak versus SAGE (Stratospheric Aerosol and Gas Experiment) III

5   and POAM (Polar Ozone and Aerosol Measurement) III, but a similar positive bias near ~28 km

6   versus HALOE (Halogen Occultation Experiment). The 'fast' product has the largest

7   overestimate at the peak of ~16% with a sharp gradient in its bias, swinging to a statistically

8   significant ~18% underestimate at 18 km. The retrieved profiles using the 2D retrieval described

9   above have a similar bias profile shape with 'fast' (Figs. 6-7) but of smaller amplitude, with a

10   ~+10% typical bias at the number density peak for the 2D retrieval and a ~10% negative bias at

11   18 km which is statistically insignificant in terms of the median (Fig. 6). The bias of the v3.0

12   product is similar to the alternative OSIRIS NO_2 products above 20 km, but between 15 and 17

13   km, there is a significant positive bias using both central tendency statistics (Figs. 6-7). In

14   contrast to 'fast' and v3.0 products, there are no altitudes in the lower stratosphere (below 24

15   km) with statistically significant average and median biases for the 1D and 2D products. This

16   conclusion is not sensitive to the use of the multiple scattering approximation used for the 1D

17   product (see Sect. 2) (not shown).

18   While Figs. 6-7 address the systematic errors of the various OSIRIS products, it is also important

19   to consider the precision of these data since a product whose biases in individual profiles average

20   to zero could still fail to adequately capture the variability. This is potentially a greater concern

21   for the v3.0 product since it relies slightly on a priori NO_2 and vertically smooths the retrieved

22   NO_2 when measurement precision is lacking. However, Haley and Brohede (2007) and Haley et

23   al. (2004) show that these are very minor concerns as the measurement response and vertical

24   resolution do not deteriorate significantly down to an altitude of 12 km. Figure 8 shows that the

25   v3.0 product captures the variability of the balloon measurements down to ~22 km as well as the

26   2D and 1D products and better than 'fast' NO_2, but then has larger scatter below 20 km than the

27   2D and 'fast'. The 'fast' retrieval benefits from more accurate forward modelling than the v3.0

28   algorithm. The reduced scatter in the lower stratosphere is unlikely to be a difference between

29   inversion approaches (MART versus the optimal estimation approach used in the v3.0 algorithm)

30   as discussed above. The 2D retrieval also may have an edge over the v3.0 algorithm by virtue of

31   using SaskTran as its forward model. There is also the specific benefit of its forward model

1 accounting for diurnal gradients in NO$_2$. This can be seen clearly between 13 and 16 km where

2 the 2D retrieval is more precise than the 1D retrieval owing to this built-in photochemical

3 modelling capability. This confirms the better precision of the 2D retrieval suggested by Fig. 3,

4 and is only expected for large SZAs (McLinden et al., 2006). Note that errors due to the neglect

5 of diurnally varying chemical gradients can alternate in sign depending on the viewing geometry

6 (McLinden et al., 2006; Brohede et al., 2007).

7 Correlation can be used as an alternative statistic to verify whether an OSIRIS product captures

8 the variability observed by coincident balloon data. It is different from the standard error statistic

9 used in Fig. 8 since multiplicative or additive biases do not affect the correlation but do affect the

10 standard error of the individual biases. The correlation is calculated over the 46 coincident

11 balloon profiles at each available altitude (Fig. 4). Figure 9 shows a general decrease in

12 correlation between OSIRIS and coincident balloon data with decreasing altitude. There is higher

13 correlation with balloon NO$_2$ data for the 2D retrieval over the 1D retrieval at the lowest

14 altitudes, consistent with Fig. 3. The correlation of the v3.0 product is comparable with the 1D

15 and 2D product down to the lowest validated altitudes, whereas the 'fast' product has generally

16 lower correlations above 22 km than the OSIRIS NO$_2$ products relying on spectral fitting.

17 Finally, since the coverage of balloon is limited to latitudes north of -22°S, Fig. 10 is included to

18 illustrate the climatological (2001-2015) vertical and meridional distribution of stratospheric

19 NO$_2$ volume mixing ratio in the southern hemisphere during austral spring. For each NO$_2$

20 vertical profile, the conversion to mixing ratio uses the local air density profile from the

21 ECMWF analysis.

22 4 Discussion

23 Next, we review and discuss the sensitivity of the retrieval to forward model parameters. There is

24 a slight sensitivity of the retrieved NO$_2$ to changes in aerosol extinction. Previous sensitivity

25 studies (Sioris et al., 2003; Haley et al., 2004) are consistent with the current findings. The scene

26 albedo in the visible can vary from <0.03 for calm ocean to almost unity for fresh snow, although

27 the NO$_2$ retrieval is, by design, insensitive to surface albedo by virtue of the high-TH

28 normalization of the radiance spectra (Sioris et al., 2003). Use of the retrieved scene albedo

29 (instead of the default value of 0.3) and of the v5.07 aerosol extinction profile further reduce

30 these sensitivities. Finally, use of OSIRIS-observed (v5.07) ozone instead of the default ozone

1. climatology in SaskTran (McPeters et al., 2007) is expected to have a minor impact on retrieved

2. NO_2 via errors in modelling the atmospheric extinction based on Sioris et al. (2007).

3. With a method that involves simulating spectra at high tangent heights for the purpose of

4. normalizing radiances simulated for tangent heights within the retrieval range, the forward model

5. must accurately compute the radiance over a large range of tangent heights. The NO_2 retrieval

6. error due to the pseudo-spherical approximation is expected to have its largest impact at low

7. altitudes, because of the vertical gradient in pseudo-spherical RTM errors (Griffioen and

8. Oikarinen, 2000). At the top of the retrieval range (40 km), errors cancel with the high altitude

9. reference.

10. While not included in Figs. 5-9, Chahine's relaxation method tends to produce sharper extrema

11. in the retrieved NO_2 profile than MART that tend to be slightly displaced vertically from those in

12. the balloon data. This may stem from the coincidence criterion of 1000 km in distance, but may

13. also relate to the ~2 km vertical sampling of OSIRIS and the 1 km altitude grid used for the

14. retrieval. If the vertical grid of the retrieval is finer than the vertical sampling, a vertically narrow

15. layer at 19 km, for example, would be retrieved as peaking at 18 km when the available radiance

16. spectra are measured at THs of 18 and 20 km. The comparison of MART and Chahine inversion

17. approaches is worth revisiting with the 1 km vertical sampling offered by the Ozone Mapping

18. Profiler Suite (Jaross et al., 2014).

19. In order to rigorously validate this new retrieval algorithm in the upper troposphere, tropospheric

20. chemistry must be added to the photochemical model used to scale the OSIRIS observations to

21. balloon local time. The reaction of NO_2 with the hydroxyl radical to form HNO_3 drives the

22. diurnal variation of tropospheric NO_2 more than N_2O_5 photolysis (Boersma et al., 2009).

23. Accurate knowledge of the seasonal variation of the OH concentration is required for modelling

24. the diurnal variation of upper tropospheric NO_2.

5 Conclusions

26. Profiles of NO_2 retrieved from OSIRIS have been improved in terms of reduced bias and scatter

27. versus the current v3.0 operational algorithm in the lower stratosphere (e.g. 15 km) as

28. determined using highly accurate balloon measurements as truth. The bias is within ~±10%

29. between 14 and 37 km.

The benefits of spectral fitting and extending the fitting window to longer wavelengths are evident at the highest altitudes where the photoelectron shot noise tends to be large relative to the NO_2 absorption signal, but also at the lowest altitudes where the retrieved profile shape is largely driven by small differences in NO_2 SCDs obtained from spectra at adjacent tangent heights. Algorithms that exploit the richness of the NO_2 absorption spectrum are shown to better capture the mid-stratospheric variability of this key constituent. The use of a fully spherical forward model is an important advantage, particularly at lower altitudes since, while the pseudo-spherical RTM errors are largest at the top of the retrieval range, the largest NO_2 retrieval errors due to the use of a pseudo-spherical RTM occur at low altitudes because a high tangent height reference is used in the retrieval.

A model capable of modelling diurnal gradients in NO_2 also helps to improve the precision of the retrieved number density profile, particularly at the lowest altitudes where the horizontal gradients in NO_2 are sharpest and where the radiance is predominantly from the near side of the limb.

Acknowledgements. This work is supported by Environment Canada through a contribution to the University of Saskatchewan. The OSIRIS project is supported by the Canadian Space Agency. Daniel Zawada (University of Saskatchewan) is acknowledged for helpful discussions regarding the high spatial resolution version of the SaskTran model. Alexei Rozanov (University of Bremen) is acknowledged for sharing his experience with the weighting-function DOAS method. Patrick Sheese (University of Toronto) provided the idea to use correlation as a statistic for validation. SALOMON-N2, SPIRALE, SAOZ, mini-SAOZ, and LPMA data were obtained from CNES/CNRS-INSU Ether web site.

References

Boersma, K. F. , Jacob, D. J., Trainic, M., Rudich, Y., DeSmedt, I., Dirksen, R., and Eskes, H. J.: Validation of urban NO_2 concentrations and their diurnal and seasonal variations observed from the SCIAMACHY and OMI sensors using in situ surface measurements in Israeli cities, Atmos. Chem. Phys., 9, 3867–3879, 2009.

1 Bourassa, A. E., Degenstein, D. A., Gattinger, R. L., and Llewellyn, E. J.: Stratospheric aerosol

2 retrieval with optical spectrograph and infrared imaging system limb scatter measurements, J.

3 Geophys. Res., 112, D10217, doi:10.1029/2006JD008079, 2007.

4 Bourassa, A. E., Degenstein, D. A., and Llewellyn, E. J.: SaskTran: A spherical geometry

5 radiative transfer code for efficient estimation of limb scattered sunlight, J. Quant. Spectrosc.

6 Radiat. Transfer, 109, 52–73, 2008.

7 Bourassa, A. E., McLinden, C. A., Sioris, C. E., Brohede, S., Bathgate, A. F., Llewellyn, E. J.,

8 and Degenstein, D. A.: Fast NO_2 retrievals from Odin-OSIRIS limb scatter measurements,

9 Atmos. Meas. Tech., 4, 965–972, 2011.

10 Brohede, S. M., Haley, C. S., McLinden, C. A., Sioris, C. E., Murtagh, D. P., Petelina, S. V.,

11 Llewellyn, E. J., Bazureau, A., Goutail, F., Randall, C. E., Lumpe, J. D., Taha, G., Thomason, L.

12 W., and Gordley, L. L.: Validation of Odin/OSIRIS stratospheric NO_2 profiles, J. Geophys. Res.,

13 112, D07310, doi:10.1029/2006JD007586, 2007.

14 Burrows, J. P., Dehn, A., Deters, B., Himmelmann, S., Richter, A., Voigt, S., and Orphal, J.:

15 Atmospheric remote-sensing reference data from GOME: 1. Temperature-dependent absorption

16 cross-sections of NO_2 in the 231-794 nm range, J. Quant. Spectrosc. Radiat. Transfer, 60, 1025-

17 1031, 1998.

18 Butz, A.: Case studies of stratospheric nitrogen, chlorine and iodine photochemistry based on

19 balloon borne UV/visible and IR absorption spectroscopy, PhD thesis, Université Paris 6, Paris,

20 pp. 254, 2006.

21 Butz, A., Bösch, H., Camy-Peyret, C., Chipperfield, M., Dorf, M., Dufour, G., Grunow, K.,

22 Jeseck, P., Kühl, S., Payan, S., Pepin, I., Pukite, J., Rozanov, A., von Savigny, C., Sioris, C.,

23 Wagner, T., Weidner, F., and Pfeilsticker, K.: Inter-comparison of stratospheric O_3 and NO_2

24 abundances retrieved from balloon borne direct sun observations and Envisat/SCIAMACHY

25 limb measurements, Atmos. Chem. Phys., 6, 1293-1314, 2006.

26 Chahine, M. T.: Determination of the temperature profile in an atmosphere from its outgoing

27 radiance, J. Opt. Soc. Amer., 58, 1634-1637, 1968.

1 Coldewey-Egbers, M., Weber, M., Lamsal, L. N., de Beek, R., Buchwitz, M., and Burrows, J. P.:

2 Total ozone retrieval from GOME UV spectral data using the weighting function DOAS

3 approach, Atmos. Chem. Phys., 5, 1015–1025, doi:10.5194/acp-5-1015-2005, 2005.

4 Degenstein, D. A., Bourassa, A. E., Roth, C. Z., and Llewellyn, E. J., Limb scatter ozone

5 retrieval from 10 to 60 km using a multiplicative algebraic reconstruction technique, Atmos.

6 Chem. Phys., 9, 6521–6529, 2009.

7 Fesen, C. G., and Hays, P. B.: Two-dimensional inversion technique for satellite airglow data,

8 Appl. Opt., 21, 3784-3791, 1982.

9 Griffioen, E., Oikarinen, L.: LIMBTRAN: A pseudo three-dimensional radiative transfer model

10 for the limb-viewing imager OSIRIS on the ODIN satellite, J. Geophys. Res., 105, 29717-29730,

11 2000.

12 Haley, C. S., Brohede, S. M., Sioris, C. E., Griffioen, E., Murtagh, D. P., McDade, I. C.,

13 Eriksson, P., Llewellyn, E. J., Bazureau, A., and Goutail, F.: Retrieval of stratospheric O_3 and

14 NO_2 profiles from Odin Optical Spectrograph and Infrared Imager System (OSIRIS) limb-

15 scattered sunlight measurements, J. Geophys. Res., 109, D16303, doi:10.1029/2004JD004588,

16 2004.

17 Haley, C. S., and Brohede, S. M.: Status of the Odin/OSIRIS stratospheric products O_3 and NO_2

18 data products, Can J. Phys., 85, 1177-1194, 2007.

19 Jaross, G., Bhartia, P. K., Chen, G., Kowitt, M., Haken, M., Chen, Z., Xu, P., Warner, J., and

20 Kelly, T.: OMPS Limb Profiler instrument performance assessment, J. Geophys. Res. Atmos.,

21 119, 4399-4412, doi: 10.1002/2013JD020482, 2014.

22 Jégou, F., Berthet, G., Brogniez, C., Renard, J.-B., François, P., Haywood, J. M., Jones, A.,

23 Bourgeois, Q., Lurton, T., Auriol, F., Godin-Beekmann, S., Guimbaud, C., Krysztofiak, G.,

24 Gaubicher, B., Chartier, M., Clarisse, L., Clerbaux, C., Balois, J. Y., Verwaerde, C., and

25 Daugeron, D.: Stratospheric aerosols from the Sarychev volcano eruption in the 2009 Arctic

26 summer, Atmos. Chem. Phys., 13, 6533–6552, 2013.

27 Kerzenmacher, T., Wolff, M. A., Strong, K., Dupuy, E., Walker, K. A., Amekudzi, L. K.,

28 Batchelor, R. L., Bernath, P. F., Berthet, G., Blumenstock, T., Boone, C. D., Bramstedt, K.,

29 Brogniez, C., Brohede, S., Burrows, J. P., Catoire, V., Dodion, J., Drummond, J. R., Dufour, D.

G., Funke, B., Fussen, D., Goutail, F., Griffith, D. W. T., Haley, C. S., Hendrick, F., Höpfner, M., Huret, N., Jones, N., Kar, J., Kramer, I., Llewellyn, E. J., López-Puertas, M., Manney, G., McElroy, C. T., McLinden, C. A., Melo, S., Mikuteit, S., Murtagh, D., Nichitiu, F., Notholt, J., Nowlan, C., Piccolo, C., Pommereau, J.-P., Randall, C., Raspollini, P., Ridolfi, M., Richter, A., Schneider, M., Schrems, O., Silicani, M., Stiller, G. P., Taylor, J., Tétard, C., Toohey, M., Vanhellemont, F., Warneke, T., Zawodny, J. M., and Zou, J.: Validation of NO_2 and NO from the Atmospheric Chemistry Experiment (ACE), Atmos. Chem. Phys., 8, 5801–5841, 2008.

Kreycy, S., Camy-Peyret, C., Chipperfield, M. P., Dorf, M., Feng, W., Hossaini, R., Kritten, L., Werner, B., and Pfeilsticker, K.: Atmospheric test of the $J(BrONO_2)/k_{BrO+NO_2}$ ratio: Implications for total stratospheric Br_y and bromine-mediated ozone loss, Atmos. Chem. Phys., 13, 6263-6274, 2013.

Llewellyn, E. J., Lloyd, N. D., Degenstein, D. A., Gattinger, R. L., Petelina, S. V., Bourassa, A. E., Wiensz, J. T., Ivanov, E. V., McDade, I. C., Solheim, B. H., McConnell, J. C., Haley, C. S., von Savigny, C., Sioris, C. E., McLinden, C. A., Griffioen, E., Kaminski, J., Evans, W. F., Puckrin, E., Strong, K., Wehrle, V., Hum, R. H., Kendall, D. J. W., Matsushita, J., Murtagh, D. P., Brohede, S., Stegman, J., Witt, G., Barnes, G., Payne, W. F., Piché, L., Smith, K., Warshaw, G., Deslauniers, D.-L., Marchand, P., Richardson, E. H., King, R. A., Wevers, I., McCreath, W., Kyrölä, E., Oikarinen, L., Leppelmeier, G. W., Auvinen, H., Mégie, G., Hauchecorne, A., Lefèvre, F., de La Nöe, J., Ricaud, P., Frisk, U., Sjoberg, F., von Schéele, F., and Nordh, L.: The OSIRIS instrument on the Odin spacecraft, Can. J. Phys., 82, 411–422, 2004.

McLinden, C. A., Olsen, S. C., Hannegan, B. J., Wild, O., Prather, M. J., and Sundet, J.: Stratospheric ozone in 3-D Models: A simple chemistry and the cross-tropopause flux, J. Geophys. Res., 105, 14 653–14 665, 2000.

McLinden, C. A., Haley, C. S., and Sioris, C. E.: Diurnal effects in limb scatter observations, J. Geophys. Res., 111, D14302, doi:10.1029/2005JD006628, 2006.

McPeters, R. D., Labow, G. J., and Logan, J. A.: Ozone climatological profiles for satellite retrieval algorithms, J. Geophys. Res., 112, D05308, doi:10.1029/2005JD006823, 2007.

Moreau, G., Robert, C., Catoire, V., Chartier, M., Camy-Peyret, C., Huret, N., Pirre, M., Pomathiod, L., and Chalumeau, G.: SPIRALE: a multispecies *in situ* balloonborne instrument with six tunable diode laser spectrometers, Appl. Opt., 44, 5972-5989, 2005.

Pommereau, J.-P. and Piquard, J.: Ozone and nitrogen dioxide vertical distributions by uv-visible solar occultation from balloons, Geophys. Res. Lett., 21, 1227–1230, 1994.

Pundt, I., Pommereau, J.-P., Chipperfield, M. P., Van Roozendael, M., and Goutail, F.: Climatology of the stratospheric BrO vertical distribution by balloon-borne UV–visible spectrometry, J. Geophys. Res., 107, 4806, doi:10.1029/2002JD002230, 2002.

Serdyuchenko, A., Gorshelev, V., Weber, M., Chehade, W., and Burrows, J. P.: High spectral resolution ozone absorption cross-sections – Part 2: Temperature dependence, Atmos. Meas. Tech., 7, 625–636, 2014.

Sioris, C. E., Haley, C. S., McLinden, C. A., von Savigny, C., McDade, I. C., McConnell, J. C., Evans, W. F. J., Lloyd, N. D., Llewellyn, E. J., Chance, K. V., Kurosu, T. P., Murtagh, D., Frisk, U., Pfeilsticker, K., Bösch, H., Weidner, F., Strong, K., Stegman, J., and Mégie, G.: Stratospheric profiles of nitrogen dioxide observed by Optical Spectrograph and Infrared Imager System on the Odin satellite, J. Geophys. Res., 108(D7), 4215, doi:10.1029/2002JD002672, 2003.

Sioris, C. E., Kurosu, T. P., Martin, R. V., and Chance, K.: Stratospheric and tropospheric NO_2 observed by SCIAMACHY: First results, Adv. Space Res., 34, 780-785, 2004.

Sioris, C. E., McLinden, C. A., Martin, R. V., Sauvage, B., Haley, C. S., Lloyd, N. D., Llewellyn, E. J., Bernath, P. F., Boone, C. D., Brohede, S., and McElroy, C. T.: Vertical profiles of lightning-produced NO_2 enhancements in the upper troposphere observed by OSIRIS, Atmos. Chem. Phys., 7, 4281-4294, 2007.

Sioris, C. E., Zou, J., McElroy, C. T., McLinden, C. A., Vömel, H.: High vertical resolution water vapour profiles in the upper troposphere and lower stratosphere retrieved from MAESTRO solar occultation spectra, Adv. Space Res., 46, 642–650, 2010.

Thomas, R. J., and Donahue, T. M.: Analysis of Ogo 6 observations of the O I 5577-A tropical nightglow, J. Geophys. Res., 77, 3557-3565, 1972.

Toon, G., Sen, B., Blavier, J.-F., Sasano, Y., Yokota, T., Kanzawa, H., Ogawa, T., Suzuki, M., and Shibasaki, K.: Comparison of ILAS and MkIV profiles of atmospheric trace gases measured above Alaska in May 1997, J. Geophys. Res., 107(D24), 8211, doi:10.1029/2001JD000640, 2002.

Vandaele, A. C., Hermans, C., Simon, P. C., Carleer, M., Colin, R., Fally, S., Mérienne, M. F., Jenouvrier, A., and Coquart, B.: Measurements of the NO_2 absorption cross-section from 42 000 cm^{-1} to 10 000 cm^{-1} (238-1000 nm) at 220 K and 294 K, J. Quant. Spectrosc. Radiat. Transfer, 59, 171-184, 1998.

Vicomte, M., and Pommereau, J. P.: Mini SAOZ : A Light UV-visible spectrometer sonde for studying convective transport in the stratosphere, Proc. 20th ESA Symposium on European Rocket and Balloon Programmes and Related Research, Hyères, France, ESA SP-700, 321-326, 2011.

Warshaw, G. D., Desaulniers, D.-L., and Degenstein, D.: Optical design and performace of the Odin UV/Visible spectrograph and infrared imager instrument, Technical Session XII, paper presented at 10th Annual AIAA/Utah State University Conference on Small Satellites, Am. Inst. of Aeronaut. and Astronaut., Logan, Utah, 1996.

Weidner, F., Bösch, H., Bovensmann, H., Burrows, J. P., Butz, A., Camy-Peyret, C., Dorf, M., Gerilowski, K., Gurlit, W., Platt, U., von Friedeburg, C., Wagner, T., and Pfeilsticker, K.: Balloon-borne Limb profiling of UV/vis skylight radiances, O_3, NO_2, and BrO: technical set-up and validation of the method, Atmos. Chem. Phys., 5, 1409–1422, 2005.

Wetzel, G., Bracher, A., Funke, B., Goutail, F., Hendrick, F., Lambert, J.-C., Mikuteit, S., Piccolo, C., Pirre, M., Bazureau, A., Belotti, C., Blumenstock, T., De Mazière, M., Fischer, H., Huret, N., Ionov, D., López-Puertas, M., Maucher, G., Oelhaf, H., Pommereau, J.-P., Ruhnke, R., Sinnhuber, M., Stiller, G., Van Roozendael, M., and Zhang, G.: Validation of MIPAS-ENVISAT NO_2 operational data, Atmos. Chem. Phys., 7, 3261–3284, 2007.

Wetzel, G., H. Oelhaf, O. Kirner, F. Friedl-Vallon, R. Ruhnke, A. Ebersoldt, A. Kleinert, G. Maucher, H. Nordmeyer, and J. Orphal, Diurnal variations of reactive chlorine and nitrogen oxides observed by MIPAS-B inside the January 2010 Arctic vortex, Atmos. Chem. Phys., 12, 6581–6592, 2012.

1   Zawada, D. J., Dueck, S. R., Rieger, L. A., Bourassa, A. E., Lloyd, N. D., and Degenstein, D.

2   A.: High-resolution and Monte Carlo additions to the SaskTran radiative transfer model, Atmos.

3   Meas. Tech., 8, 2609-2623, 2015.

1   Table 1. Main features of OSIRIS NO_2 algorithms compared in this work.

	v3.0 operational	'fast'	1D, 2D, 3D
Wavelength range (nm)	435-451	438-450	435-477
Number of spectral pixels	41	13	107
RT model	LIMBTRAN	SaskTran (1D)	SaskTran (1D, 2D, 3D)
Inversion scheme	Optimal estimation	MART (0.5: 0.3: 0.2)	MART (0.6: 0.3: 0.1)
Cloud detection	Yes	No	Yes
NO_2 absorption cross-sections	220 K (Vandaele et al., 1998)	(Burrows et al., 1998)	220, 298 K (Vandaele et al., 1998)
Interpolation of fitted cross-section to effective T	No	yes, using local ECMWF temperature at each TH	yes, using local ECMWF temperature at each TH

2 Table 2. Summary of validation data based on OSIRIS coincidences. The minimum relative

3 uncertainty is reported on the native vertical grid. Vertical resolution is quoted or calculated for

4 an altitude of 16 km. The vertical resolution is provided by Butz (2006) for LPMA and DOAS,

5 Weidner et al. (2005) for mini-DOAS, available at http://mark4sun.jpl.nasa.gov/m4data.html for

6 MkIV, and calculated for limb occultation for the SAOZ-type instruments, including

7 SALOMON-N2 (Jégou et al., 2013) assuming vertical resolution equal to the vertical extent of

8 the solar disk at the tangent point. Uncertainties are for a 1 km vertical grid, except for SPIRALE

9 (0.005 km) and mini-DOAS (2 km).

Instrument	Number of coincidences	Relative uncertainty (%)	Vertical Resolution (km)	Average lower altitude (km)	Average upper altitude (km)
MkIV	6	2	~2	9	38
SPIRALE	4	<1	0.005	16	33
SALOMON-N2	1	15	2	15	33
DOAS asc	3	5	1.5	9	29
DOAS limb	4	<1	1.5	13	32
mini-DOAS	2	4	2	8	29
LPMA asc	1	10	6	10	33
LPMA limb	4	10	5	15	31
Mini-SAOZ	1	4	2	15	29
SAOZ-BrO asc	1	2	1	3	36
SAOZ-BrO SS	1	4	2	22	37
SAOZ asc/desc	9	<1	1	6	29
SAOZ limb	9	<1	2	11	29
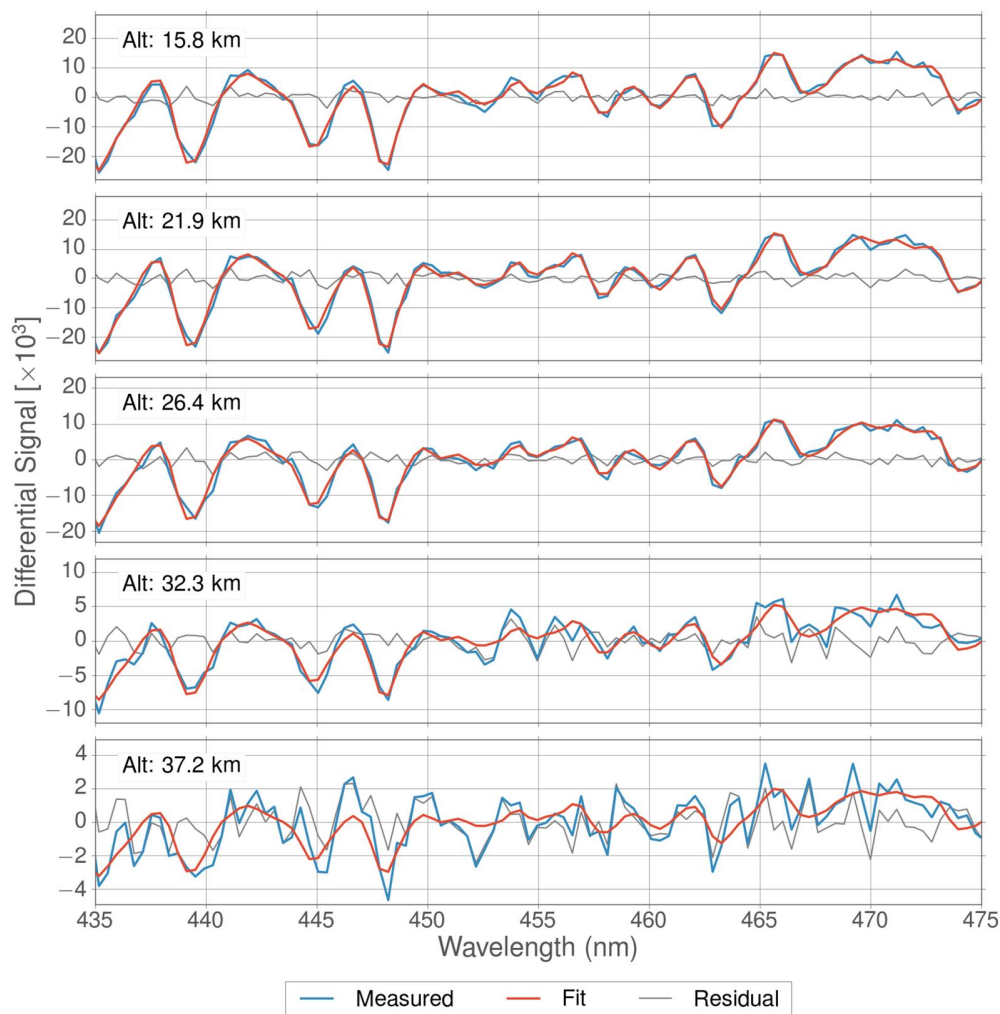
3 Figure 1. Measured and fitted differential optical depth (DOD) as a function of tangent height

4 ('Alt') in the spectral window used for NO_2 retrieval. The residual is calculated as measured

5 DOD – fitted DOD.
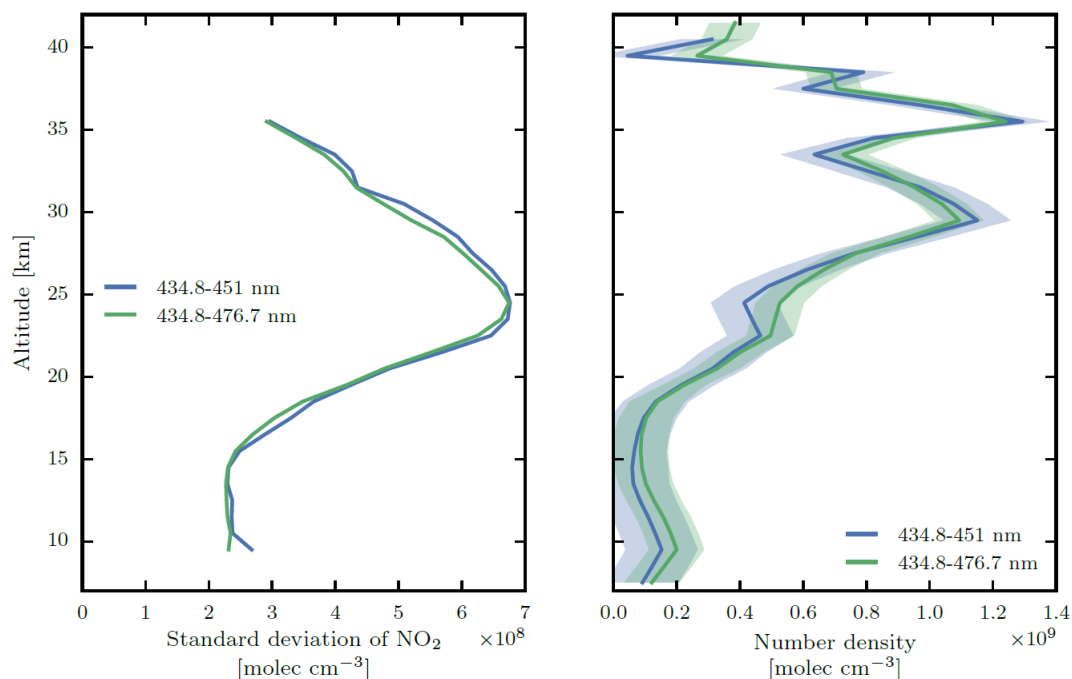
Figure 2. (left) Comparison of the standard deviation of the NO_2 number density profiles
retrieved with the algorithm described above using the default window (435-477 nm) versus the
fitting window used in the OSIRIS v3.0 operational algorithm (Haley and Brohede, 2007), (right)
Comparison of a single NO_2 profile retrieved from scan 20 of orbit 60346 with the algorithm
described above using the default window (435-477 nm) versus the fitting window used in the
OSIRIS v3.0 operational algorithm.
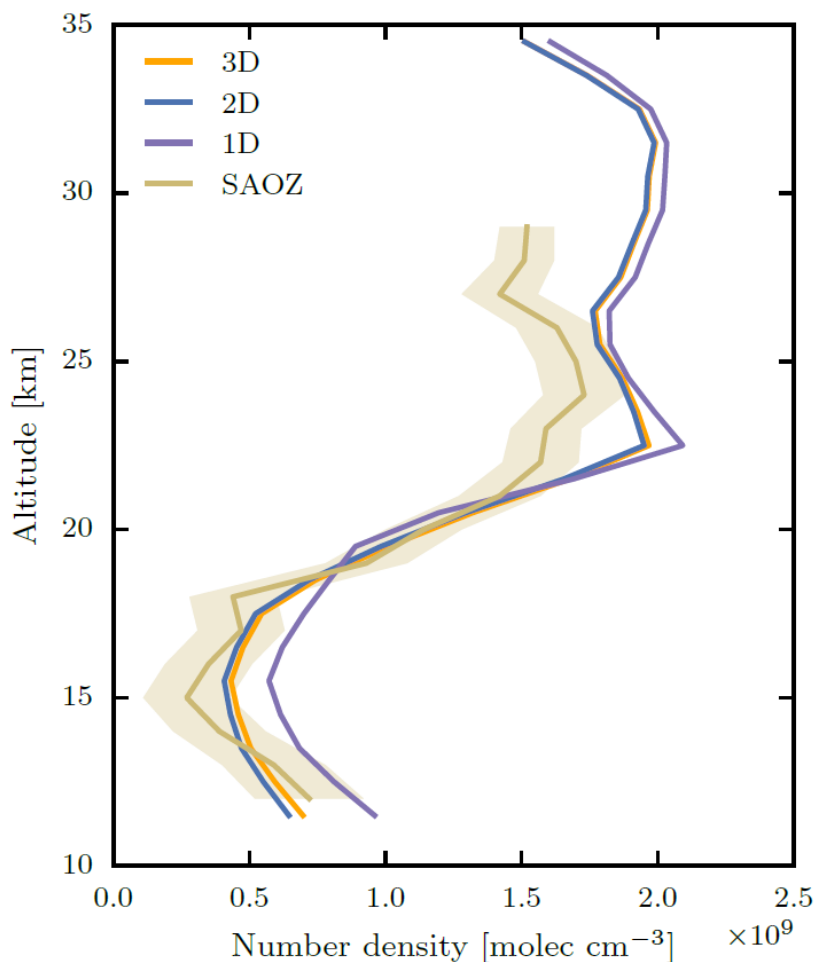
Figure 3. NO$_2$ profile retrieved from scan 44 of orbit 16011 using the 1D, 2D, and 3D retrievals, all converted to sunset (tangent point SZA=90°), the local time of coincident SAOZ measurements. OSIRIS is on the day side with SZA=86.6° (pm) and an azimuth difference angle of 99° such that the far side of the limb is closer to the terminator.
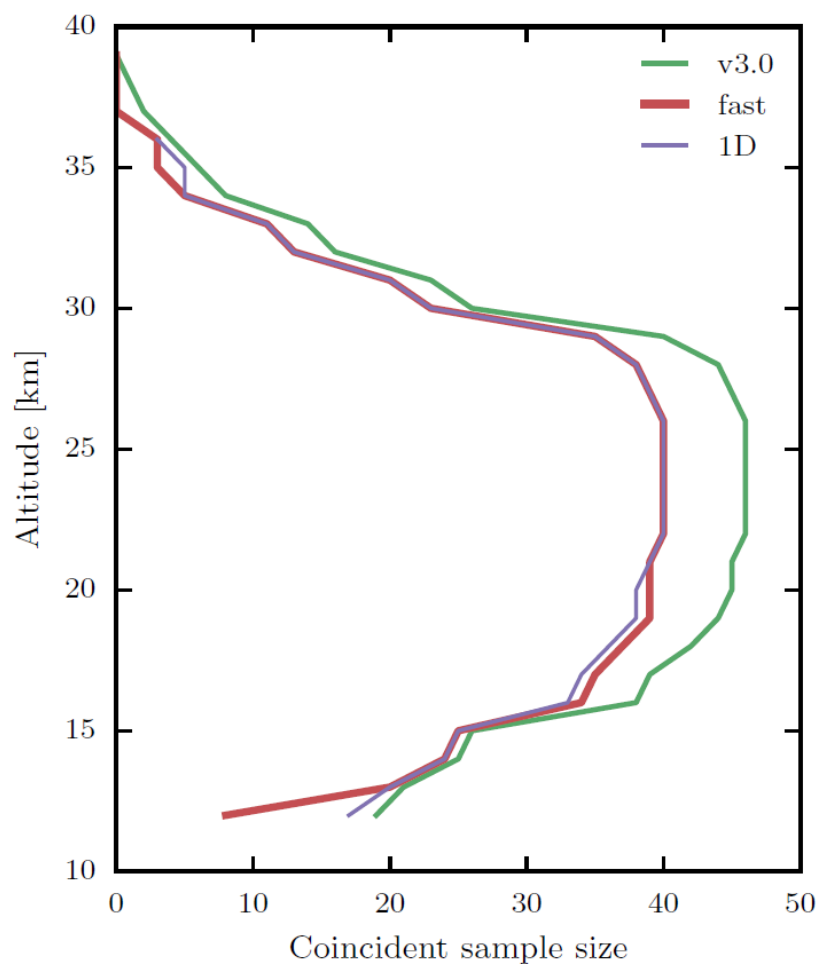
2   Figure 4. Sample size of coincident balloon data versus altitude and as a function of retrieval

3   algorithm.
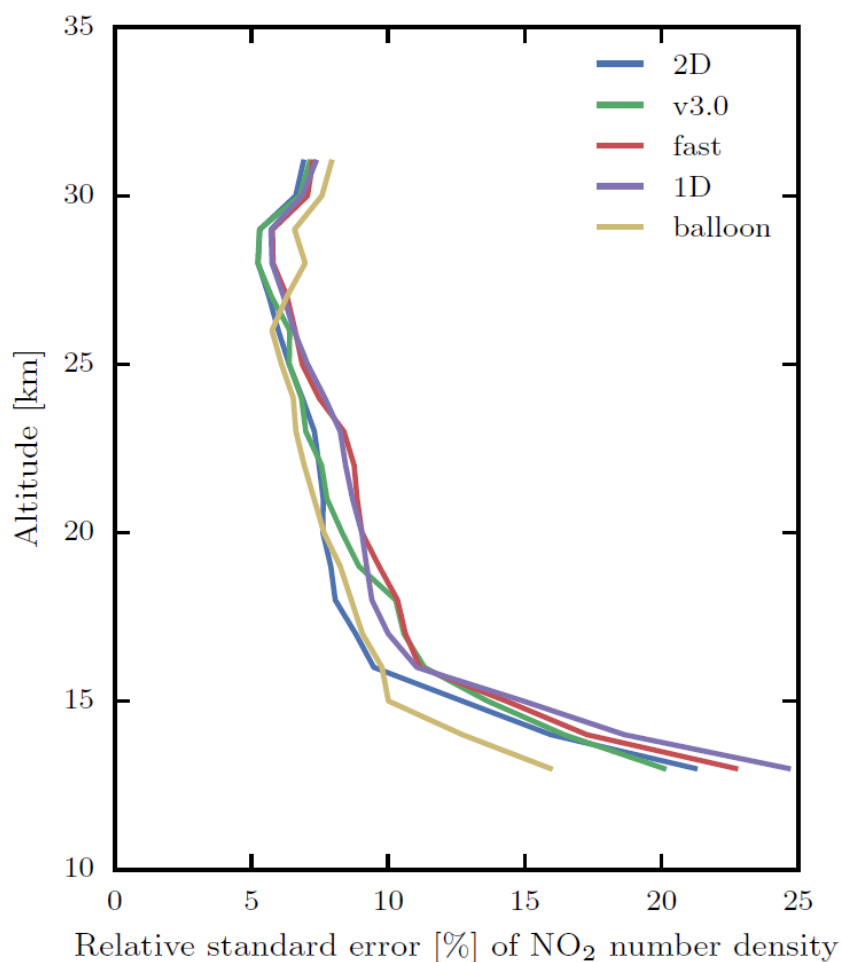
Figure 5. Relative standard error of coincident NO_2 profiles. Note that OSIRIS profiles have been scaled to various local times of the balloon measurements which adds random error to the OSIRIS profiles due to random variations between the photochemical model atmosphere and true atmosphere.
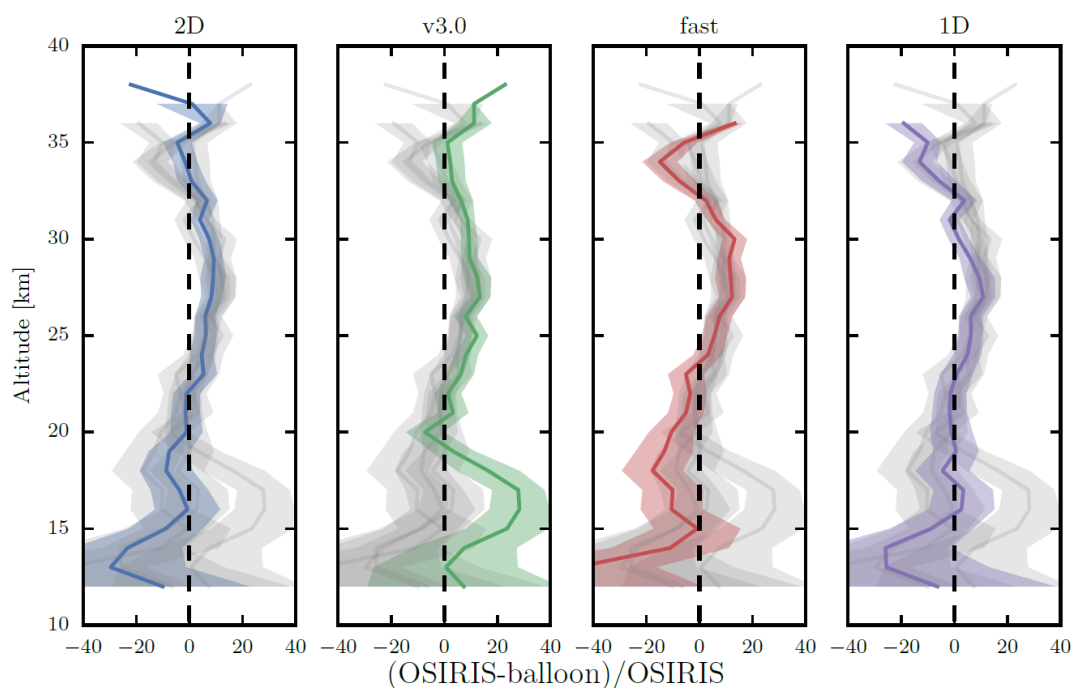
Figure 6. Median of individual biases versus balloon data. The error bar shows ±1 standard error

of the median NO_2 bias profile. The median and standard error of the individual biases are

converted to relative quantities by dividing by the corresponding median OSIRIS NO_2 profile

(scaled to balloon local time). The relative median bias profiles for the other three algorithms are

shown in gray for comparison.
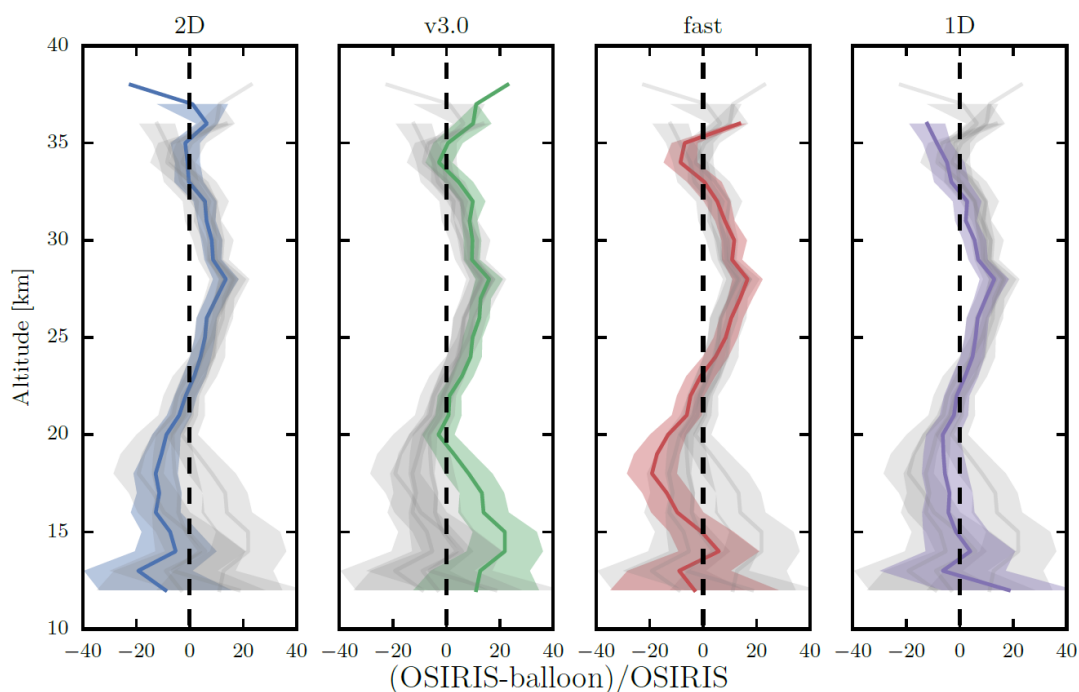
2   Figure 7. same as Fig. 6, but the bias is an average over individual differences between OSIRIS

3   and balloon correlative data. The average and standard error of the individual biases are

4   converted to relative quantities by dividing by the corresponding average OSIRIS NO_2 profile

5   (scaled to balloon local time).
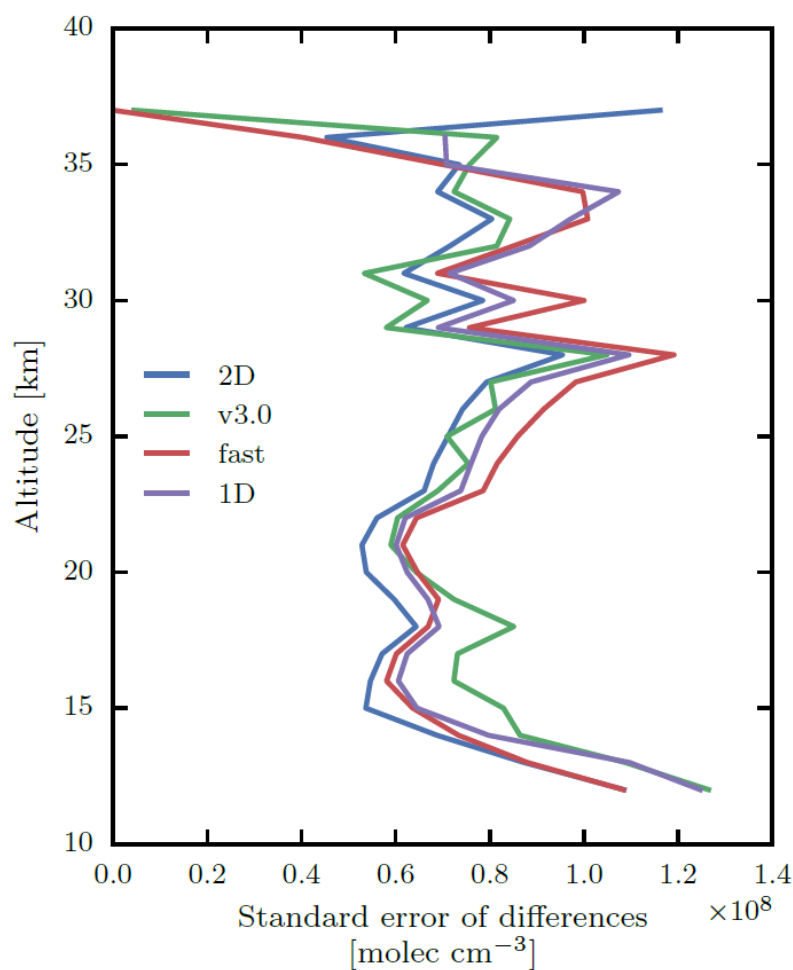
2   Figure 8. Standard error of the individual biases relative to balloon correlative data for different

3   OSIRIS NO$_2$ products. The curves here correspond to the half-widths of the error bars in Figs. 6-

4   7.
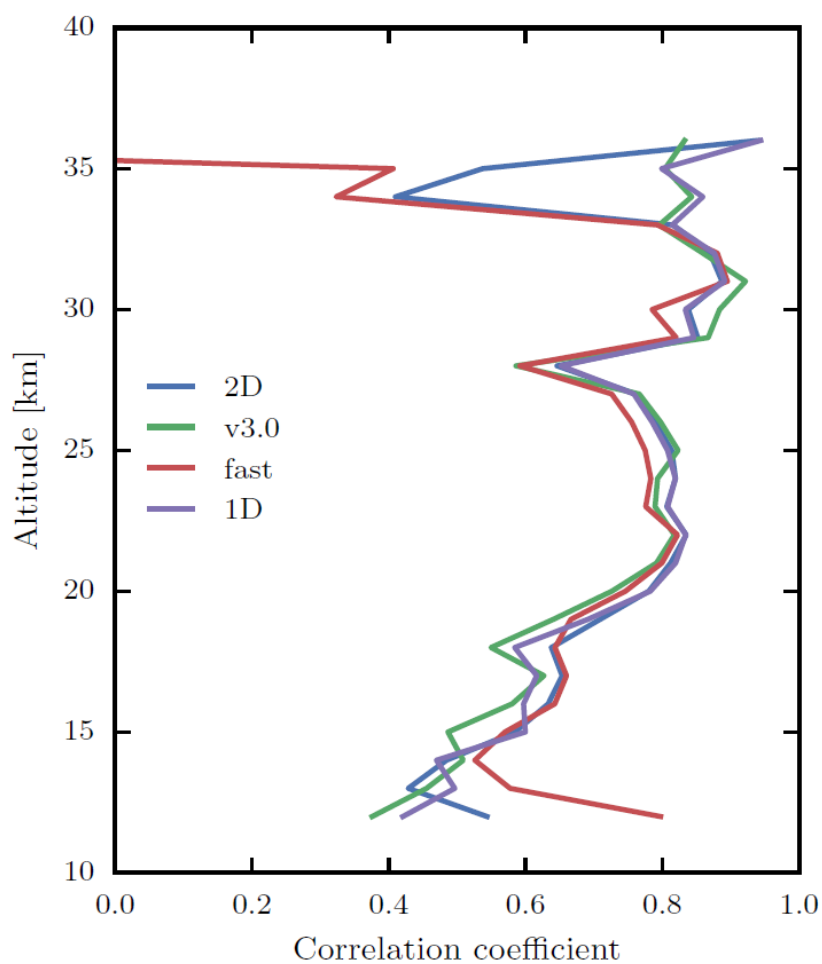
2   Figure 9. Correlation between various OSIRIS NO$_2$ products and the balloon validation dataset.
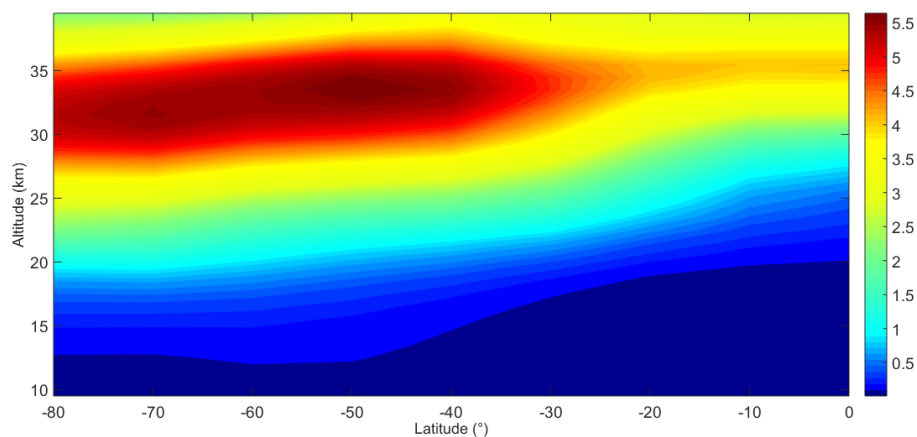
2   Figure 10. Climatological map of zonal mean NO_2 volume mixing ratio (ppb) with 10°

3   latitudinal binning and 1 km vertical binning centered at altitudes between 9.5 and 39.5 km for

4   November (2001-2014).